J Solid State Eletrochem (2004) 8: 244–251
DOI 10.1007/s10008-003-0433-5

ORIGINAL PAPER

**Merlin C. E. Bandeira · Franci D. Prochnow
Lúcia K. Noda · Norberto S. Gonçalves
Isolda Costa · Hercílio G. de Melo · Joe A. Crayston
César V. Franco**

Electroreductive polymerization of *trans*-[$RuCl_2(vpy)_4$] on Nd-Fe-B magnets: electrochemical impedance spectroscopy interpretation, Raman spectroscopy, X-ray photoelectron spectroscopy and scanning electron microscopy analysis

Received: 29 July 2002 / Accepted: 25 June 2003 / Published online: 6 January 2004

Abstract The electropolymerization of *trans*-[$RuCl_2(vpy)_4$] (vpy = 4-vinylpyridine) monomer on Nd-Fe-B magnets was studied by electrochemical impedance spectroscopy (EIS). Impedance diagrams obtained during the polymerization process were used to monitor film formation. The EIS results gave insight into the electrochemical phenomena occurring at the magnet surface as the polymerization process progressed. The film structure and morphology were also studied by X-ray photoelectron spectroscopy, scanning electron microscopy and Raman spectroscopy. The Raman spectroscopy results showed that the polymerization takes place at the vinyl groups of the monomer and also that the redox polymer structure is very similar to that of the monomer. The ratio of the intensity of the XPS peaks for fluorine (from the electrolyte PF_6^-) and ruthenium present in the film showed that the polymer on Nd-Fe-B contained an equal proportion of Ru^{2+} and Ru^{3+}, indicating that part of the film is positively charged, i.e. $\{[RuCl_2(vpy)_4]^+\}_n$.

Keywords Electrochemical impedance spectroscopy · Poly{*trans*-[$RuCl_2(vpy)_4$]} film · Raman spectroscopy · X-ray photoelectron spectroscopy

M. C. E. Bandeira · F. D. Prochnow · L. K. Noda
N. S. Gonçalves · C. V. Franco (✉)
Departamento de Química-CFM,
Universidade Federal de Santa Catarina,
Campus Trindade, LEC, 88040-900
Florianópolis, SC, Brazil
E-mail: franco@qmc.ufsc.br

I. Costa
IPEN/CNEN, CCTM,
SP, Brazil

H. G. de Melo
Departamento de Engenharia Química,
EPUSP, SP, Brazil

J. A. Crayston
School of Chemistry,
University of St. Andrews,
KY16 9ST St. Andrews,
Fife, Scotland, UK

Introduction

The monomer *trans*-[$RuCl_2(vpy)_4$] was first synthesized in our laboratory in 1995, and its synthesis and electrochemical behaviour have been reported in the literature [1]. The reductive electropolymerization of this complex has been used in our group to coat noble substrates, such as Pt and Pd, and also as an alternative in the corrosion protection of active materials such as Nd-Fe-B magnets, Fe-Ni alloys and stainless steels [1, 2, 3, 4, 5]. Since the monomer electropolymerization potential is cathodic, active substrates can be coated, without electro-oxidation. Electrocoating from monomers with redox centres is an alternative strategy in electrocatalysis and corrosion protection, modifying the electrode behaviour due to the low oxidation state of immobilized transition metals in the polymeric matrix.

Nd-Fe-B magnets show outstanding magnetic properties, and owing to their high-energy product, applications of this kind of magnet have increased in the last decade [6, 7]. Their main applications include consumer electronics, computer peripherals, acoustics, office automation, and magnetic resonance imaging. However, their poor corrosion resistance limits their use for some applications. In recent years, efforts have been concentrated in increasing their corrosion resistance through the application of surface coatings [8].

Poly{*trans*-[$RuCl_2(ypy)_4$]} films have been investigated as an alternative surface coating for Nd-Fe-B magnets. The electropolymerization mechanism has also

been studied to find the best electrocoating conditions in order to obtain a better performance of these coatings against the corrosion process [9]. Raman spectroscopy studies associated with electrochemical methods have been used to produce information on the kinetic processes and reaction mechanisms [10].

Electrochemical impedance spectroscopy (EIS) is a strategic analytical method widely employed in basic and applied electrochemistry, as well as in the material science field [11]. However, it should be used in tandem with other techniques, such as SEM, AFM and XPS [11, 12, 13, 14]. In the present work, results on the electropolymerization process of *trans*-[$RuCl_2(vpy)_4$] redox polymer on Nd-Fe-B magnets are reported. The polymerization process was followed using in situ EIS during the polymerization process and ex situ Raman spectroscopy, XPS and SEM to characterize the redox polymer on the Nd-Fe-B substrate. For comparison, some analyses were also carried out on Pt and Au substrates.

Experimental

Reagents and synthesis

Commercially available analytical grade reagents were employed throughout this work. $RuCl_3.3H_2O$ (Johnson-Matthey) and 4-vinylpyridine (vpy) (Aldrich) were used without further purification. The synthesis method used to produce the ruthenium blue solution and *trans*-[$RuCl_2(vpy)_4$] is described elsewhere [1].

Sample preparation

Nd-Fe-B sintered magnets (Sumitomo) with an exposed area of 0.95 cm^2 were ground with 500-grit emery paper and degreased with ethanol. Subsequently, the magnet samples were coated with poly{*trans*-[$RuCl_2(vpy)_4$]} films. The film electropolymerization was carried out by cyclic voltammetry (CV) between 0.2 and −2.8 V vs. SCE at 50 mV s^{-1}. The monomer concentration was 5 mmol cm^{-3} in CH_3CN/CH_2Cl_2 (4:1) and the electrolyte used was 0.1 mol cm^{-3} $TBAPF_6$ (tetrabutylammonium hexafluorophosphate) [2]. All experiments were performed at room temperature (22 ± 2 °C) and the electrolyte was quiescent.

Electrochemical impedance spectroscopy

EIS tests were carried out using a frequency response analyser (Solartron SI 1255) coupled to a potentiostat (EG&G 273A), and controlled by the supplied electrochemical impedance software. The measurements were obtained at room temperature during the film growth (in situ) at −2.8 V vs. SCE in the frequency range between 100 kHz and 100 mHz at 10 points per decade, and with a perturbation sign amplitude of 10 mV (r.m.s.). A classical three-electrode arrangement was used to perform these experiments, with SCE and Pt wire as the reference and counter electrodes, respectively.

Raman spectroscopy

Raman spectra were obtained using a Renishaw Raman System 3000 equipped with a CCD, using the 632.8 nm line of a He-Ne laser (Spectra-Physics model 127). The laser was focused onto the electrode surface by means of a microscope (Olympus BH2T) and the laser power was kept at 3 mW.

Electrochemical tests

The electrochemical experiments were performed using a PAR 263 potentiostat. The Nd-Fe-B magnet working electrode was placed in a Teflon holder and mounted in a Teflon cell containing the electrolyte. The reference and counter electrodes were silver and platinum wires. The electropolymerization was carried out under the same conditions described above, except for the electropolymerization on the gold electrode which was done in potentiostatic mode at −2.2 V vs. SCE for 15 min (the polymerization potential is shifted anodically on gold). After the electropolymerization process, the working solution was removed and the film on the electrode was rinsed with acetonitrile and dried with nitrogen. Raman spectra of the formed film were then obtained. Raman spectra of the film obtained on a gold electrode (also mounted on a Teflon holder) and of the neat complex were also obtained for comparison purposes.

X-ray photoelectron spectroscopy measurements

XPS data were obtained with a VG ESCALAB II XPS spectrometer, using Al-Kα radiation. The electrons were collected using an electrostatic focusing lens and the analyser was a single-channel hemispherical type. The base pressure was 2×10^{-10} mbar, and samples were loaded via an independently pumped fast-entry lock. All detailed spectra were collected using a pass energy of 20 eV in intervals of 0.05 eV. The charged shifted peaks were corrected by an internal calibration standard. The F 1s binding energy was considered as 689.40 eV [15]. All other peaks in the spectrum had the binding energy corrected according to the charge shift of the F 1s internal standard. Analyses of films polymerized on Pt and on Nd-Fe-B magnets at a fixed potential (−2.8 V vs. SCE) during 1200 s (Pt) and 2400 s (Nd-Fe-B) were performed.

Results and discussion

EIS measurements during film polymerization

Bode phase angle plots obtained at different polarization cycles are presented in Fig. 1a. Two different time constants associated with a capacitive behaviour are clearly distinguishable in this figure, in accordance with the model proposed by several authors to explain the impedance behaviour of thin redox polymer films [16, 17, 18]. Regarding the origin of the high-frequency time constant, in the literature it was first ascribed to the electron transfer process at the polymer/solution interface due to redox-active species present in the solution [16]. Later, Vorotynstev et al. [17] further improved this model for blocked electrodes, attributing the high-frequency capacitive loop to charge transfer, either ionic, at the polymer/solution interface, or electronic, at the polymer/metal interface. The ionic charge transfer at the polymer/solution interface would be ensured by the counter-ions present in the background electrolyte, and no redox-active species was considered to be present in the solution [17].

The models proposed by Deslouis et al. [16] and by Vorotynstev et al. [17], although explaining well the impedance characteristics of some redox polymer systems, were based on simplified assumptions such as the absence of electroactive species in the background electrolyte in the former [16] and absence of redox-active species in the latter [17]. These models, however, cannot

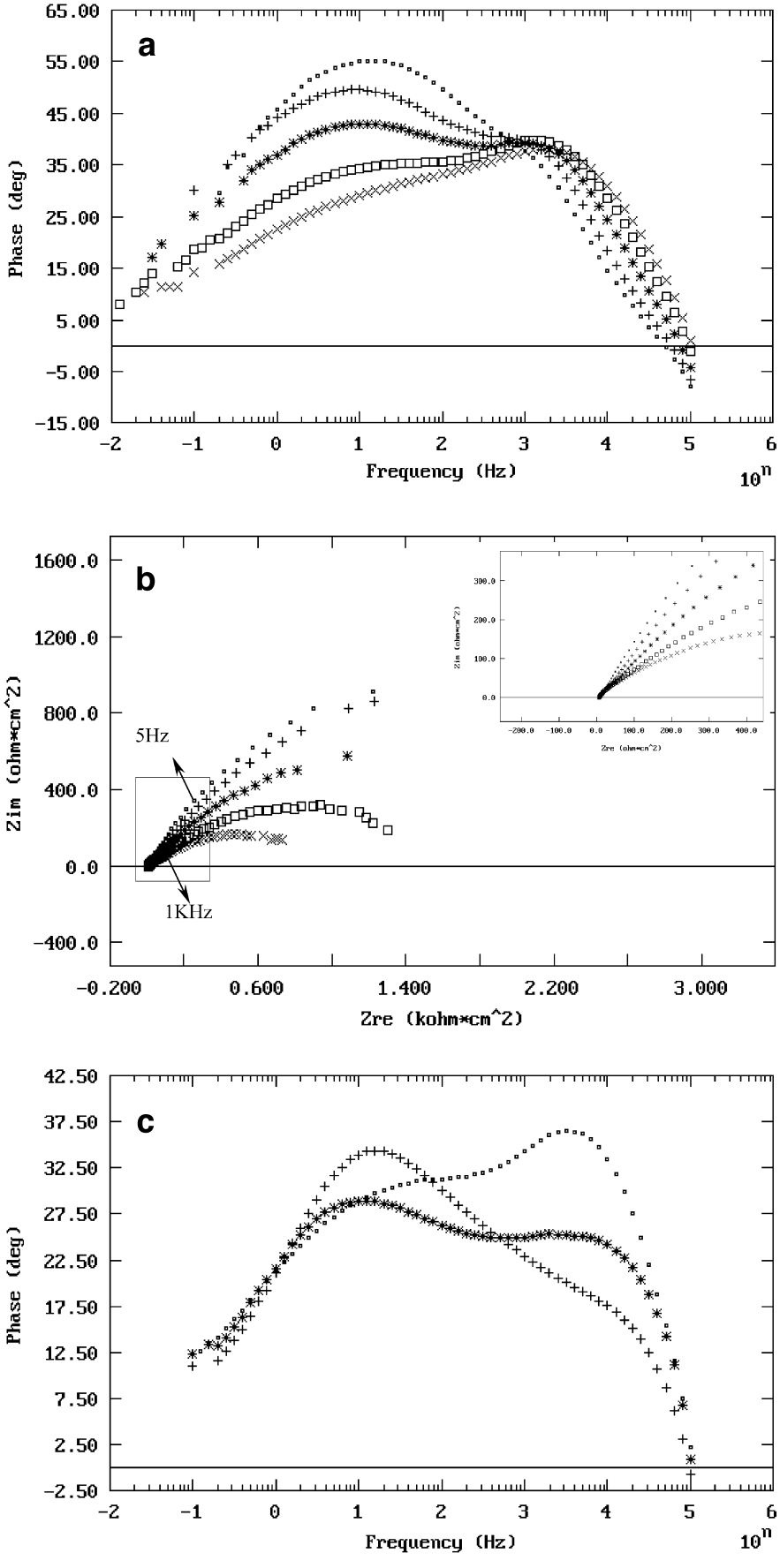

Fig. 1a, b EIS of *trans*-$[RuCl_2(vpy)_4]$ polymerization in CH_3CN/CH_2Cl_2 (4:1) at increasing polymerization times: *dots*, after 1 min (2 cycles); *plusses*, after 2.5 min (5 cycles); *asterisks*, after 5 min (10 cycles); *squares*, after 7.5 min (15 cycles); *crosses*, after 10 min (20 cycles). Frequency range: 100 kHz to 100 mHz; $E = -2.8$ V vs. SCE. (**a**) Bode diagrams and (**b**) Nyquist diagrams; *inset* shows a zoom in the 100 kHz to 5 Hz region. (**c**) Bode diagrams obtained: *dots*, after 12.5 min (25 cycles); *plusses*, after 15 min (30 cycles); *asterisks*, after 17.5 min (35 cycles) of polymerization

fully explain the origin of the high-frequency loop of Fig. 1, since in the polymerization medium used here, contributions of both the counter-ions of the background electrolyte (PF_6^-) and of the redox-active species to the total impedance are possible. In a more recent work, Vorotynstev et al. [18] considered the situation where both electronic and ionic interfacial fluxes occur at the polymer/solution interface. In their work, the high-frequency loop was credited to a parallel combination of the ionic and electronic charge transfer resistances at the polymer/solution interface, the former due to counter-ions present in the background electrolyte and the latter due to the formation of radical anions [18]. No contribution of the charge transfer at the metal/polymer interface to the total impedance of the film was envisaged, since this phenomenon was considered fast by the authors. The explanation of Vorotynstev et al. [18] is perhaps more relevant to explain the origin of the high-frequency loop presented in the diagrams of Fig. 1, as it describes a situation closer to the experimental conditions used in this work.

The second time constant presented in Fig. 1, in the intermediate- to low-frequency range, can be also explained by a parallel combination of phenomena occurring at the metal/solution interface and within the polymer. The former could be some cathodic reaction, due to the extremely negative potential at which the electropolymerization reaction takes place. This reaction would occur in parallel with the whole polymerization process, and would take place on metal sites not yet covered by the polymer. On the other hand, the latter could be the electron transfer reaction between the metal redox sites in the polymer where the polymerization process has already started, as proposed by Gabrielli et al. [19]. It must be emphasized that, owing to the relatively high low-frequency limit employed here, 100 mHz, the diagrams presented in Fig. 1 may not represent all of the interfacial faradaic phenomena. However, impedance results are only meaningful when steady-state conditions are fulfilled, thus limiting the frequency range investigated in impedance experiments. The short time necessary to reach the low-frequency limit used in this study (100 mHz) indicates that the flattening of the diagrams is not due to system evolution.

The evolution of the polymerization process can be clearly followed in the diagrams presented in Fig. 1a. For diagrams obtained after 1 min and 2.5 min of polymerization, although a small shoulder is present at high frequencies, the dominant processes occur at moderate- to low-frequency ranges and likely reflect the cathodic reaction occurring at the metal/solution interface. This behaviour indicates that the polymerization process only takes place in a period following the monomer adsorption process. More evidence about adsorption on the electrode before the film polymerization was found from Raman and EQCM studies [9]. As the polymerization time increases, the high-frequency time constant becomes more defined and shifts towards higher frequencies, indicating a more effective polymerization reaction. However, the phase angle related to this time constant progressively decreases as the polymerization cycles increase. This behaviour might suggest the existence of a diffusion-controlled process within the solution, owing to the formation of a monomer-depleted zone near the electrode surface, as the polymerization reaction progresses. Deslouis et al. [16], in their model to explain the impedance behaviour of redox polymers in solutions containing a redox couple, have already envisaged the existence of a diffusion layer near the electrode surface. To avoid the monomer-depleted zone, these authors used a rotating disk electrode [16]. It is also worth mentioning that the Nd-Fe-B magnet used was produced by powder metallurgy (sintered magnet) and therefore the substrate is a porous material, as Fig. 2 shows, and this could probably lead to the growth of porous redox polymer films. Indeed, Saliba-Silva [20], using quantitative metallography, has determined that porosities are approximately 15% of the surface area of the magnets used in this study. The joint action of these two factors may cause the appearance of small phase angles and of highly depressed loops in the Nyquist diagrams, as can be seen in Fig. 1a and Fig. 1b.

The evolution of the impedance diagrams at moderate to low frequencies with polymerization time, presented in Fig. 1a, can be better understood if we take into account the occurrence of cathodic reactions at the potential where the impedance experiments were performed. As already stated, these reactions would take place at the polymer-free surface and would occur in parallel with the polymerization process. Figure 3 shows a generic equivalent circuit that could represent a simplified physical model of the whole system, where *Rs* is the solution resistance, *Rpol* the resistance of the charge transfer reactions at the polymer/solution interface, *Cpol* the capacity of the polymeric film, *W* represents diffusion-controlled processes within the polymer, *Zpol* is the faradaic impedance within the polymer, *Ru* is the resistance of the polymer-free magnet surface (maybe *Rct*), *Cu* is the capacity of the polymer-free magnet surface

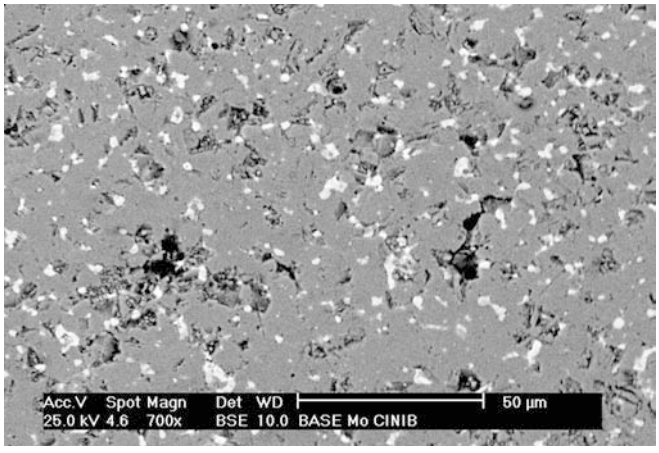

Fig. 2 SEM image of sintered Nd-Fe-B magnet

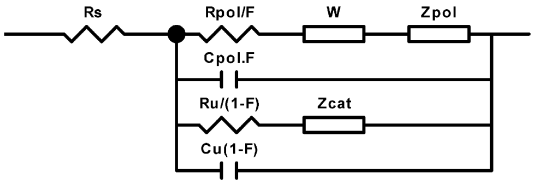

Fig. 3 Simplified equivalent circuit of the magnet surface considering the existence of polymer coated (*pol*) and uncoated (*u*) areas. The definitions of the circuit element symbols are given in the text

(maybe *Cdl*), *Zcat* is the faradaic impedance of the cathodic reaction, and *F* is the area fraction covered with polymer ($0 \leq F \leq 1$).

From the analysis of Fig. 3 it can be seen that if the area fraction covered with polymer is small, *F* approaches zero, and all the current would flow through the part of the equivalent circuit related to the polymer-free surface. On the other hand, as the polymerization reaction proceeds, *F* increases and the current would flow through the two branches of the equivalent circuit. In the limiting case, the surface would become completely covered by the polymer ($F = 1$), and the whole current would flow through the polymeric layer. This kind of reasoning, presenting parallel pathways for electrochemical reactions, has already been used by several authors to simulate data of passive metals under pitting corrosion processes [21, 22]. In this case, *F* represents the area fraction on which pitting occurs.

It must be emphasized that the equivalent circuit presented in Fig. 3 by no means represents an accurate picture of the actual interfacial phenomena. The complexity and even the existence of the *Zpol* and *Zcat* elements depend on how complex are the faradaic phenomena taking place at the uncovered and covered surfaces. Moreover, the existence of parallel interfacial reactions at the polymer/solution interface, giving rise to the high-frequency loop [18], was deliberately neglected in the equivalent circuit. A full simulation is beyond the scope of this paper.

The analysis of the diagrams presented in Fig. 1a and Fig. 1b, bearing in mind the equivalent circuit of Fig. 3, can help to shed some light on the phenomena related to the time constant at moderate to low frequencies. As can be seen in Fig. 1a, the Bode phase angle diagram obtained after 1 min of polarization shows a small shoulder in the high-frequency region followed by a well-defined peak. The corresponding Nyquist diagram (Fig. 1b) displays only one capacitive loop. It can be assumed that initially there was no compact polymer film on the electrode surface, but only a few polymerization sites. The low-frequency phase angle at this stage would be mainly representative of the cathodic processes taking place at the bare electrode surface, even though some reactions linked to the existence of the polymer could occur at the few sites where the nucleation process has already started. In this case, *F* would tends towards zero and all the current would flow through the branch of the equivalent circuit related to the cathodic reactions. The low phase angle related to this loop can be likely attributed to the porosity of the electrode. No corrosion reaction was envisaged due to the cathodic potential employed in the polymerization process. It is worth mentioning that, in some cases, flattening of the impedance diagrams is associated with non-steady-state conditions. However, for the frequency range investigated in this work, the time span necessary to obtain the impedance diagrams was approximately 10 min. During this period it is unlikely that the current drift (the experiments were performed under potentiostatic conditions) would be high enough to invalidate the results in the low-frequency region. Moreover, Saliba-Silva [20], when studying the phosphating process for corrosion protection of Nd-Fe-B magnets, has verified the important contribution of the porosity to the impedance response of this material.

As polymerization progresses and the polymeric film grows more compact and thicker, the high-frequency capacitive loop becomes more pronounced. At the same time, the diameter of the capacitive loop at intermediate to low frequencies progressively diminishes. In this case the *F* factor would increase with time, and the impedance response of the polymer would increasingly dominate the process.

So, as the polymer layer becomes more compact, the low-frequency capacitive loop would represent only the phenomena related to the redox polymer. In this case the existence of diffusion-controlled processes within the polymer film [18, 19] could explain the increasing depression of the low-frequency capacitive loop with the progress of the polymerization process, and the shift of the phase angle peak to lower frequencies, cf. Fig. 1a. Figure 1c presents the Bode diagrams obtained after 12.5, 15 and 17.5 min of polymerization. It can be seen in the Bode phase angle corresponding to 15 min of polymerization that the peak in the medium- to low-frequency range becomes more pronounced, while the one at high frequencies, presumably related to the phenomena at the polymer/solution interface, almost disappears. This behaviour could have been caused by discontinuities in the film, resulting from several processes, such as cracks, polymeric chain degradation or low adherence to the substrate, all of them leading to the exposure of the bare magnet surface, with the consequent decrease of the *F* value. Two time constants are clearly seen again after 17.5 min of polymerization. According to our interpretation, this last diagram suggests that the polymerization process was not interrupted, regardless of the film damage.

Raman measurements

The Raman spectrum of the neat complex presented in Fig. 4 shows several bands at 1012, 1057, 1200 and 1604 cm^{-1}, assigned to pyridine ring modes (ν_{12}, νC–H, νC–X and ν_{8a}). A weak band at ca. 1626 cm^{-1} assigned to ν(C = C), from the non-polymerized vinyl groups, and

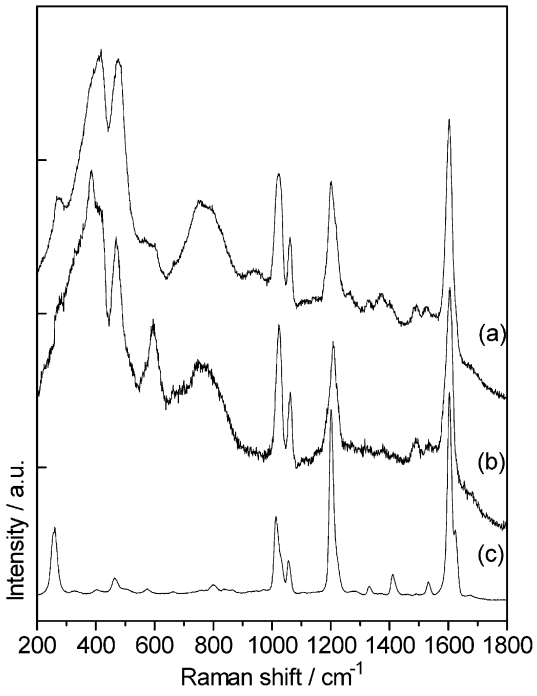

Fig. 4 Raman spectra of the film grown on (**a**) the gold electrode, (**b**) the NdFeB magnet and (**c**) the neat complex

a low-frequency band at ca. 250 cm^{-1}, assigned to ν(Ru–N), were also identified [23].

The ex situ Raman spectrum of the gold electrode, obtained after 15 min of contact with the working solution, under a potential of −2.2 V vs. SCE, does not show the band at ca. 1626 cm^{-1} [ν(C=C)]. This indicates that the polymerization process takes place by the vinyl groups [24]. Three broad bands are observed in the low-frequency region (ca. 420 cm, 480 cm and 750 cm^{-1}), probably due to some ruthenium oxide formed on the electrode surface [25]. The Raman spectrum of the film formed on the Nd-Fe-B magnet (conditions: cyclic voltammetry between 0.2 and −2.8 V vs. SCE at 50 mV s^{-1}) is similar to that obtained from a film grown on the gold electrode, except for differences in the broad bands at the low-frequency region. This result suggests that the film structure, and consequently the growth mechanism, is similar for both substrates.

XPS measurements

The XPS analyses were carried out on films which were electropolymerized on Pt and Nd-Fe-B magnets. The binding energies of the elements found in each sample are presented in Table 1. According to the literature [26, 27, 28], the binding energy of Ru $3d_{5/2}$ is strongly affected by the ligand coordinated to the metallic centre. A range of binding energies for Ru^{2+} complexes have been reported which vary from 279.50 to 281.80 eV, for $[Ru(en)_3]ZnCl_4$ and $[Ru(NH_3)_5CO](PF_6)_2$, respectively [27]. The Ru^{3+} complexes showed higher binding energies than those observed for Ru^{2+}, and the energies are also affected by the coordination environment. In some cases the Ru $3d_{3/2}$/C 1s overlap can be a significant problem in the measurement of the C 1s energy. Since it is very important to measure accurately the Ru $3d_{5/2}$ binding energy, we followed the procedure described in the literature [27], calculating Δ, where $\Delta = E$(C 1s−Ru $3d_{5/2}$), in order to determine the Ru oxidation state in the films analysed (Table 1). The value of Δ for the as-grown film on Pt is close to that expected for the complex in the Ru(II) state. Using the graph correlating the redox potential of Ru(II) complexes with Δ [27], we predict a Δ value of 4.9, which is close to that observed. It is difficult to predicted the value of Δ for the Ru(III) state; values of 2.5–3 have been reported for complexes in quite different coordination environments [27, 28]. Our complex contains Cl ligands which may act as very efficient π-donors to Ru(III). Nevertheless, it is clear that a lower value of Δ suggests a greater proportion of Ru(III) present in the film. On this basis the amount of Ru^{3+} varies in the order Nd-Fe-B > Pt(ox) > Pt.

Since the Ru $3d_{5/2}$ binding energies observed do not give a quantitative estimate of the amount of Ru^{3+} present, it was decided to analyse the area of the F 1s and Ru $3d_{5/2}$ peaks to confirm the proposed hypothesis about the Ru oxidation state. The ratio F:Ru is expected to vary as a function of the film oxidation state, since during oxidation the PF_6^- counter-ion from the electrolyte is incorporated to maintain the film's electroneutrality. Hence, the amount of F 1s in the film is directly proportional to the film oxidation state. Fluorine was observed in all three samples studied (Table 2). The F:Ru ratio in the film on the Nd-Fe-B magnet was 10 times higher than the ratio observed to the film on Pt, and 5 times higher than the film on Pt(ox). According to these results the film electropolymerized on the Nd-Fe-B magnet exists as an

Table 1 The XPS parameters of $\{[RuCl_2(vpy)_4]\}_n$ films

Substrate	Binding energies/eV (±0.1)					Δ = *E* (C 1s−Ru $3d_{5/2}$)
	Cl 2p	Ru $3d_{5/2}$	C 1s	N 1s	F 1s	
Nd-Fe-B	196.2	285.1	289.5	404.3	689.4	4.4
Pt(ox)[a]	203.4	283.5	288.0	403.2	689.4	4.5
Pt[a]	200.7	283.3	288.1	402.8	689.4	4.8

[a]Both films were polymerized under the same conditions, but the Pt(ox) was electrochemically oxidized after polymerization

Table 2 XPS peak areas in $\{[RuCl_2(vpy)_4]\}_n$ films

Substrate	Ru $3d_{5/2}$	F 1s	F:Ru	% Ru^{3+}
Nd-Fe-B	2373	12481	5.2:1	46
Pt(ox)[a]	2475	4631	2.3:1	27
Pt[a]	2673	1357	0.5:1	7.7

[a]Both films were polymerized under the same conditions, but the Pt(ox) was electrochemically oxidized after polymerization

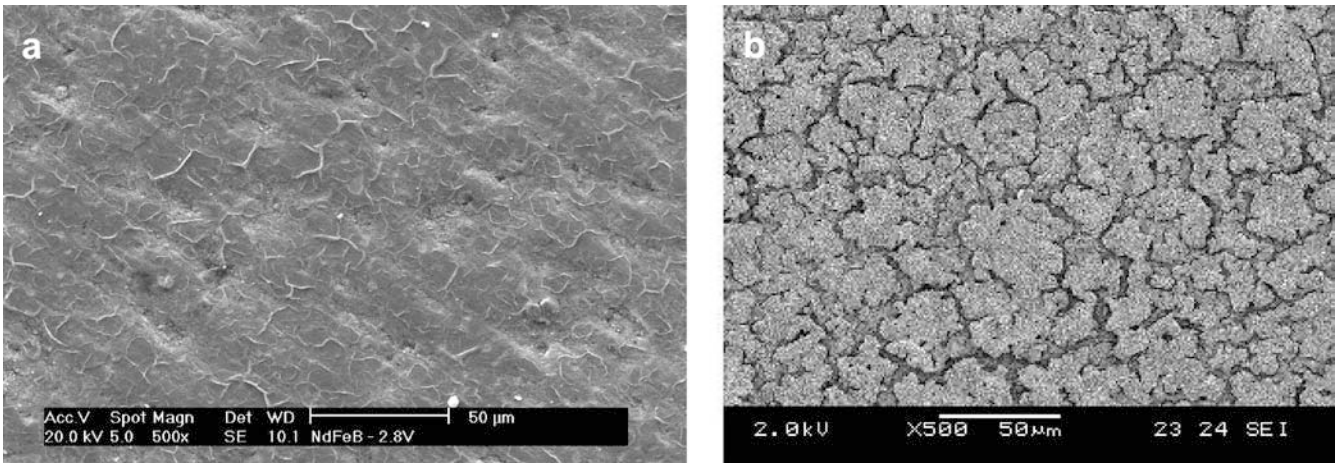

Fig. 5a, b SEM image of $\{trans\text{-}[RuCl_2(vpy)_4]\}_n$ film on the Nd-Fe-B magnet. Electropolymerization was carried out via (**a**) CV between 0.2 and −2.8 V at 50 mV s^{-1} for 25 cycles and (**b**) FP at −2.8 V vs. SCE for 2400 s

approximately equal mixture of Ru^{3+} and Ru^{2+} species, while in the other films the Ru^{2+} species was the major component.

These data give clear evidence of the strong influence of the Nd-Fe-B substrate on the film oxidation state. In those films polymerized on a Pt surface, a strong resistance to electrochemically oxidize the ruthenium from Ru^{2+} to Ru^{3+} was found. In contrast, film oxidation was spontaneous on the magnets. Our hypothesis is that one of the active phases of this alloy has been dissolved in solution in the form of Nd^{3+} ions during the polymerization process. Several authors have studied the electrochemical behaviour of Nd-Fe-B magnets in different media [20, 29, 30] and a common feature is that the Nd-rich phase, which constitutes approximately 7.3% of the total surface area of the magnet [20], is much more active than the rest of the surface, mainly composed of the Fe-rich ϕ phase. So the reduction of Nd^{3+} ions is likely to occur during the polymerization process, oxidizing Ru^{2+} ions to Ru^{3+} in the film. Indeed, Pourbaix diagrams indicate that the redox potential $E(Nd^{3+}/Nd)$ is close to the potential used for polymerization (−2.8 V vs. SCE).

Scanning electron microscopy

The films electropolymerized by CV and at a fixed potential (FP) showed some morphological differences [2], the former presenting more cracks and other defects, as Fig. 4 illustrates. In fact, the basic morphology is almost the same; however, it is strongly influenced by the polymerization time. During the FP polymerization, the film grows fast and thickens quickly, forming the cracks shown in Fig. 5. One possible explanation for this behaviour lies in the low conductivity of the film, since at this stage the film is more positively charged (as was shown by the XPS results). It is also possible that this morphology is a consequence of the low adherence of the polymer on the film itself.

Conclusions

EIS measurements permit the monitoring of the electroreductive polymerization of $trans\text{-}[RuCl_2(vpy)_4]$ on Nd-Fe-B magnets. From analysis of the impedance diagrams, together with a proposed equivalent circuit representing the whole interface, it was possible to gather some information about the predominant reactions in the different polymerization stages. According to the EIS diagrams, in the first few minutes of polymerization, monomer adsorption rather than polymerization was the controlling process for the polymerization. At this stage the main impedance response is ascribed to cathodic reactions taking place at the bare magnet surface, and the diagrams would be characterized by only one time constant in the intermediate- to low-frequency range. As polymerization progressed, the high-frequency time constant became more defined and the phase angle decreased, suggesting that the polymerization is spread over the entire magnet surface. Also the existence of a diffusion-controlled process within the polymer is evidenced during this latter polymerization stage. Raman spectra showed that the redox polymer has a structure similar to that of the monomer. It also confirmed that polymerization takes place via the vinyl groups. Films polymerized on gold and Nd-Fe-B magnets had similar structures and the polymerization mechanism on both substrates might be very similar. XPS results showed that the films on Nd-Fe-B magnets contain significant amounts of Ru^{3+}. This probably arises from the film acting as a reducing agent, reducing some of the Nd^{3+} ions dissolved in the solution during polymerization, and acting as a sacrificial anode.

Acknowledgements The authors would like to thank CAPES (Coordenação de Aperfeiçoamento de Pessoal e Ensino Superior) for financial support. The authors are also grateful to Laboratório de Espectroscopia Molecular (LEM-IQUSP) for the use of the Raman

spectroscopy facility and to Dr. Steve Francis for XPS analysis at St. Andrews University.

References

1. Franco CV, de Moraes VN Jr, Mocellin F, Paula MMS (1998) J Mater Chem 8:2049
2. Bandeira MCE, Prochnow FD, Costa I, Franco CV (1999) J Corros Sci Eng 2, paper 4 (http://www.cp.umist.ac.uk/JCSE/vol2/Paper4/v2p4.html)
3. Bandeira MCE, Prochnow FD, Costa I, Franco CV (2001) Key Eng Mater 189–191:673
4. Prochnow FD, Bandeira MCE, Costa I, Franco CV (2000) Proc simpósio matéria 2000: materiais & energia, p 84 (in Portuguese)
5. Sobral AVC, Ristow W Jr, Domenech SC, Franco CV (2000) J Solid State Electrochem 4:417
6. Fidler J, Schrefl T (1996) J Appl Phys 79:5029
7. Kim AS, Camp FE (1996) J Appl Phys 79:5035
8. Nakayama T, Sato F, Hanaki A (Kobe Steel Ltd, Japan) (1993) Patent DETAILS REQUIRED (country, patent number, etc.)
9. Bandeira MCE (2001) PhD thesis, UFSC, Brazil (in Portuguese)
10. Faria DLA, Temperini MLA, Sala O (1999) Quim Nova 22:541 (in Portuguese)
11. Lyons MEG (1994) Electroactive polymer electrochemistry, part 1: fundamentals. Plenum Press, New York, pp 164–195
12. Ren X, Pickup PG (1997) J Electroanal Chem 420:251
13. Aramaki K (1999) Corros Sci 41:1715
14. Yan LJ, He YF, Lin HC, Wu WT (1999) Acta Physico-chim Sinica 15:726
15. Nefedov VI, Gati D, Dzhurinskii BF, Sergushin NP, Salynya V (1975) Russ J Inorg Chem 20:2307 (http://www.lasurface.com)
16. Deslouis C, Musiani MM, Tribollet B (1989) J Electroanal Chem 264:37
17. Vorotyntsev MA, Daikhin LI, Levi MD (1994) J Electroanal Chem 364:37
18. Vorotyntsev MA, Deslouis C, Musiani MM, Tribollet B, Aoki K (1999) Electrochim Acta 44:2105
19. Gabrielli C, Haas O, Takenouti H (1987) J Appl Electrochem 17:82
20. Saliba-Silva AM (2001) PhD thesis, IPEN, Brazil (in Portuguese)
21. Mansfeld F, Wang Y (1995) Mater Sci Eng A 198:51
22. Xingwen Y, Chunan C, Zhiming Y, Derui Z, Zhongda Y (2000) Mater Sci Eng A 284:56
23. Paula MMS, Konzen M, Seifriz I, Gonçalves NS, Spoganicz B, Franco CV (1999) J Bioinorg Chem 76:153
24. Noda LK, Sala O (2000) Spectrochim Acta A 56:145
25. Liu HL, Yoon S, Cooper SL, Cao G, Crow JE (1999) Phys Rev B 60:R6980
26. Denesevich P, Abruña HD, Leidner CR, Meyer TJ, Murray RW (1982) Inorg Chem 21:2153
27. Shepherd RE, Proctor A, Henderson WW, Myser TK (1987) Inorg Chem 26:2440
28. Brant P, Stephenson TA (1987) Inorg Chem 26:22
29. Bala H, Pawlowska B, Szymura S (1990) J Magn Magn Mater 87:1255
30. Bala H, Pawlowska B, Szymura S, Rabinovich Y (1998) Br Corros J 33:37